Rational Design of Single-Component White-Light Emissive Molecular Copper Clusters

Alexia Rocheteau, Lanig Lemeur, Marie Cordier, Michaël Paris, Jean-yves Mevellec, Camille Latouche, Hélène Serier-Brault, Sandrine Perruchas

Rational Design of Single-component White-Light Emissive Molecular Copper Clusters

*Alexia Rocheteau,[a] Lanig Lemeur,[a] Marie Cordier,[b] Michaël Paris,[a] Jean-Yves Mevellec,[a] Camille Latouche,[a,c] Hélène Serier-Brault[a] and Sandrine Perruchas[a]**

[a] Nantes Université, CNRS, Institut des Matériaux de Nantes Jean Rouxel, IMN, F-44000 Nantes, France.
Phone: (+33) (0)2 40 37 63 35. E-mail: sandrine.perruchas@cnrs-imn.fr

[b] Univ. Rennes, CNRS, ISCR (Institut des Sciences Chimiques de Rennes) - UMR 6226, F-35000 Rennes, France.

[c] Institut Universitaire de France (IUF) Paris F-75005, France.

Abstract.

The development of low-cost and earth-abundant phosphors for substituting expensive noble metals and toxic lead materials, is currently of major importance for sustainable solid-state lighting technologies. Hybrid copper halide materials are currently receiving considerable attention due to their unique and diverse structural and photophysical properties combined to their low cost and toxicity. This article reports the rational design of copper iodide compounds for developing single-component white light emitters. By a ligand engineering strategy, the energy layout of the molecular clusters could be adjusted and the variation in the relative intensity of two emission bands could be obtained, enabling white light to be emitted. Temperature dependence of this dual-emission feature also allows high contrast luminescence thermochromism. Thanks to their good solubility properties, the studied copper iodide clusters have been successfully incorporated within organic polymer leading to polymer materials with processability suitable for applications development. Therefore, the potential applicability of these composite materials has been demonstrated in various fields as luminescence ratiometric thermometers, single-component emitters for phosphor-converted white-light emitting diodes and as ink for anticounterfeiting properties. This study highlights the power of the ligand design strategy to develop high potential multifunctional materials based on light-emitting copper materials.

Keywords. Copper cluster, phosphine ligand, white luminescence, thermochromism, light-emitting diode, ratiometric thermometry, anticounterfeiting.

1. Introduction.

In today's world of digital technologies, it is essential to reduce one of the most important electricity consumption coming from light-emitting devices. Although luminescent materials with enhanced performance are required for high-quality lighting and displays technologies, they are first and foremost highly demanded for energy savings. Besides, there is an urgent need to consider sustainable and ecological aspects in solid-state lighting technologies. For this reason, the development of low-cost, earth-abundant phosphors for substituting expensive noble-metal-based materials is currently of major importance.[1–6] In regards to phosphor-converted white-light emitting diodes (PC-WLEDs), lead halide perovskites have been recognized as most promising phosphors due to their excellent physical properties. However, the toxicity of lead and structural instability are significant obstacles to commercial developments.[7,8] In this context, copper-based materials and in particular hybrid copper(I) halides,[9–11] are currently receiving considerable attention due to their unique and diverse photophysical properties combined with their modest cost and low toxicity.[12,13] Their potential applications in scintillators,[14–18] light-emitting diodes,[19–24] and advanced stimuli-responsive materials,[25–28] have been indeed reported. Because of their chemical and thermal stabilities, copper iodide materials in particular, constitute solid alternatives for phosphor-converted white LEDs applications. Although several white emitting copper iodide compounds have recently been reported by combination with organic cations,[29–34] the study of single-component white phosphors based on neutral compounds with broad-band emission appear of great interest to avoid the difficulties of controlling the mixing of different luminophores. The only few reported examples of such single-molecular emitters, prompts the exploration of new white phosphors based on copper iodide materials.[35–37]

Among the remarkable structural diversity of copper iodide compounds that originates from the versatile coordination chemistry of Cu(I) able to accommodate any types of ligands, the polymetallic complexes exhibit particularly rich photophysical properties.[38,39] The intriguing cubane cluster of $[Cu_4I_4L_4]$ (L = organic ligand) formula, is emblematic of this. This compact molecular structure is built on four copper and four iodide atoms which alternatively occupy the vertices of a distorted cube with ligands completing the fourfold coordination sphere of Cu(I).[40,41] These clusters usually present high photoluminescence quantum yield and chemical photostability,[42–47] making them promising for a wide range of applications but especially giving them relevant characteristics as single-component white-light-emitting phosphors. Examples of $[Cu_4I_4L_4]$ clusters displaying white emission are extremely rare[35,37] and the rational design of such single component white emitters along with the comprehension of the underlying photophysical processes continue to pose challenges. Indeed, two main limitations of these $[Cu_4I_4L_4]$ clusters emerge being their emission energy range and their poor processability mainly due to low solubility. Indeed, for the fabrication of efficient luminescent devices, solution-based processes are preferred because of the low stability during vacuum deposition of these compounds, but these processes require good solubility in conventional solvents that is not easily encountered for these compounds. Additionally, polymer materials are more easily handled and more suitable for practical applications and the homogeneous dispersion of the phosphors within polymeric matrix requires also good solubility properties. The other limitation is their emission that usually lies in the visible range mainly from green to yellow color. The obtaining of white emission with these clusters is usually reached by mixing with additional commercial phosphors but the assembly can be complex. Getting

white emission from these single component clusters would require to enlarge their panel of emission colors by modification of their emissive states' layout. Red-emitting $[Cu_4I_4L_4]$ clusters exist,[43] but only very few blue emissive clusters at room temperature are known.[37,48,49] One of them was reported by us and was obtained by coordination of the copper atoms with phosphine ligands bearing trifluoromethyl (CF_3) groups.[48] The stabilization of the blue emission at room temperature is render possible by the strong electron withdrawing character of the ligands. Based on this result, we thought that thanks to a ligand engineering strategy, by adjusting the electron withdrawing character of the ligand, we could obtain both blue and yellow emission at room temperature, leading to the targeted white emission.

In this article, we report the successful achievement of this strategy for designing single-component white-light copper iodide emitters. Indeed, the energy layout of the system could be tuned by ligand engineering, allowing the relative intensity of the two emissions to be varied and white light emission properties to be achieved. Temperature dependence of this dual-emission characteristic also leads to high contrast luminescence thermochromism. Thanks to their solubility in a wide range of solvents, the studied clusters have been successfully incorporated into organic polymer leading to polymer materials that are easily processed and suitable for applications development. The potential applicability of these composite materials has thus been demonstrated for luminescence ratiometric thermometry and for white-light emitting diodes as single-component phosphors. Anti-counterfeiting properties were additionally evaluated. This study highlights the relevance of the ligand design strategy to achieve specific target properties that enable the development of high potential multifunctional materials based on cost-effective light-emitting copper materials.

2. Results and Discussions.

2.1. Synthesis and structural characterizations.

To coordinate the $[Cu_4I_4L_4]$ clusters, the chosen ligands are phenyl-phosphine derivatives functionalized with trifluoromethyl CF_3 groups. The ligands differ by their number of CF_3 groups at the para position of the phenyl rings, from one to three per ligand. Accordingly, the electron withdrawing character increases with the number of CF_3 groups, as illustrated in Figure 1.

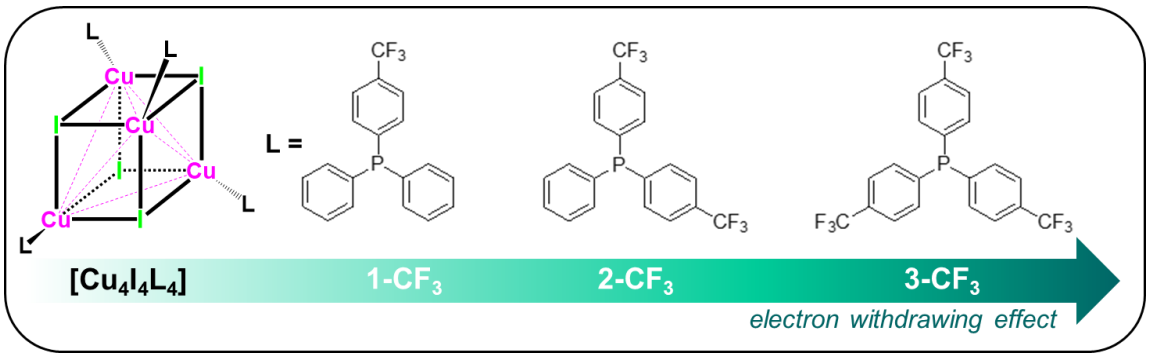

Figure 1. General representation of the studied $[Cu_4I_4L_4]$ clusters **C-CF₃** (L = phosphine ligand).

Chart 1. Designation of the studied clusters **C-CF₃**.

$[Cu_4I_4(PPh_2(C_6H_4\text{-}CF_3))_4]$	**1-CF₃**
$[Cu_4I_4(PPh(C_6H_4\text{-}CF_3)_2)_4]$	**2-CF₃**
$[Cu_4I_4(P(C_6H_4\text{-}CF_3)_3)_4]$	**3-CF₃**

The clusters **C-CF$_3$** (Chart 1) were synthesized in solution from CuI and the corresponding ligand (details in experimental section in SI). While the ligand of **3-CF$_3$** is commercially available, we have synthesized the mono- and di-substituted ligands of **1-CF$_3$** and **2-CF$_3$** respectively, according to literature reports.[50] The clusters were obtained as white crystalline powders in good yields (> 80 %), precipitated by adding a nonsolvent to the reaction medium. Single-crystals were obtained by slow solvent diffusion methods (details in experimental section). Note that the three complexes are readily soluble in most of the common organic solvents, given them good processability properties. Elemental analysis results confirm the [$Cu_4I_4L_4$] formula of the clusters with presence of solvent molecules for **2-CF$_3$** from recrystallization (C_6H_{14}). Liquid ^{31}P and ^{1}H and ^{19}F NMR analyses agree with the ligand formula and its coordination to the copper atom (details in SI). Thermogravimetry analyses indicate thermal stability of the compounds up to 200 °C (Figure S17).

Single crystal X-Ray diffraction (SCXRD) analysis at 150 K indicate that **1-CF$_3$** crystallizes in the triclinic *P*-1 space group and **2-CF$_3$** in the trigonal *P*-3 one (experimental details in SI and Table S1). The crystal structure of **3-CF$_3$** was already reported in the *P*-1 space group.[48] The molecular structures of the clusters are depicted in Figure 2. **C-CF$_3$** all present the cubane geometry with four copper and four iodide atoms forming a distorted cube. The phosphine ligands are coordinated to the copper atoms leading to the pseudo-tetrahedral $PCuI_3$ coordination environment. The CF_3 groups present disorder in the three structures. In **1-CF$_3$**, two ligands are disordered with two positions for the F atoms and also two positions for the CF_3 groups on two different phenyl groups of the same ligand. In **2-CF$_3$**, one ligand is disordered with the CF_3 group positioned on the three phenyl groups, in accordance with the 3-fold axis passing through the P-Cu bond of this ligand. Solvent molecules were detected in **2-CF$_3$** and could be identified as hexane from elemental analyses. In **3-CF$_3$**, two CF_3 groups are disordered with two positions for one of the three F atom. The unit cell contents are shown in Figure S1. The structures can be described as assemblies of columns of clusters running along the *a* axis. In all three structures, multiple short H···F and F···F intermolecular contacts (< 3 Å) take place between the clusters.

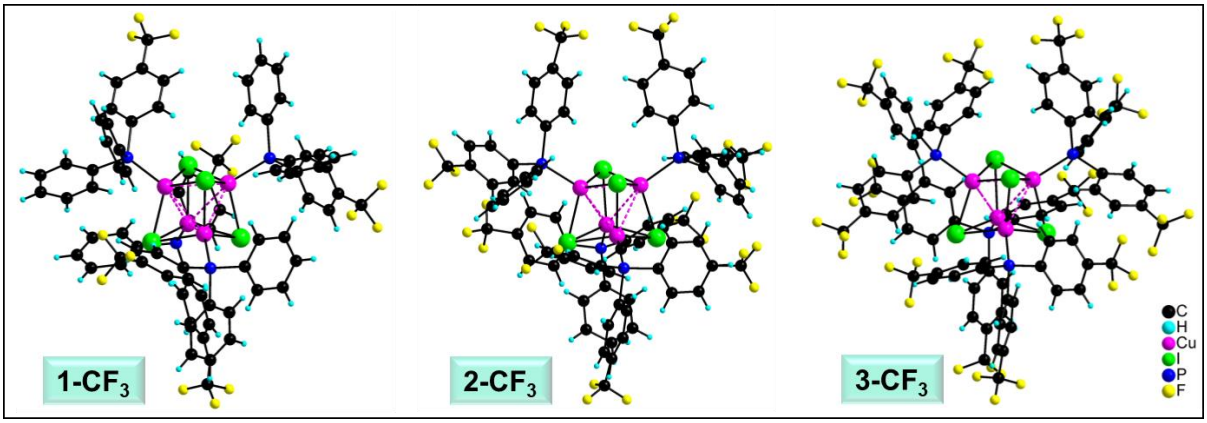

Figure 2. SCXRD molecular structures of **C-CF$_3$** clusters. The Cu-Cu interactions are represented in dotted pink lines. The disordered CF_3 groups are not shown for clarity.

Selected bond lengths and angles of the clusters are reported in Table 1. The Cu-P and Cu-I bond distances and the I-Cu-I angle values are all comparable and within the range of reported values for cubane-type copper iodide clusters coordinated by phosphine ligands.[42,45,51] The six Cu-Cu distances are in the common 2.8-3.2 Å range and are comparable with the sum of the van der Waals radii of copper

of 2.80 Å. This indicates occurrence of cuprophilic interactions (d^{10}-d^{10} bonding) in the **C-CF$_3$** compounds.[52,53] The Cu_4 tetrahedron volume are all comparable but is slightly larger for **1-CF$_3$** with value of 3.18(1) Å^3 compared with 3.10(1) and 3.02(1) Å^3 of **2-CF$_3$** and **3-CF$_3$**, respectively. The larger standard deviation in the I-Cu-I angle values for **1-CF$_3$** is also indicative of a more distorted cubane geometry compared with that of **2-CF$_3$** and **3-CF$_3$** (Table 1). PXRD (Powder X-ray diffraction) analyses are in accordance to SCXRD data and confirms the purity and homogeneity of the powder samples (Figure S2).

Table 1. Selected bonds lengths and angles in **C-CF$_3$** at 150 K.

Compound	**1-CF$_3$**	**2-CF$_3$**	**3-CF$_3$**
Cu-Cu (Å)	2.8801(14)	2.9030(12)*3	2.8849(8)
	2.9193(14)	3.0540(13)*3	2.9053(9)
	2.9388(14)		2.9267(9)
	3.0249(13)		2.9605(9)
	3.1535(14)		3.0137(8)
	3.1719(14)		3.0267(9)
mean	*3.0148(14)*	*2.9785(13)*	*2.9530(9)*
standard-deviation	*0.124*	*0.083*	*0.058*
Cu_4 (Å^3)	*3.18(1)*	*3.10(1)*	*3.02(1)*
Cu-I (Å)	2.6532(11)	2.6515(8)*3	2.6244(7)
	2.6545(11)	2.6737(9)*3	2.6478(7)
	2.6597(11)	2.6860(6)*3	2.7608(7)
	2.6623(11)	2.6953(9)*3	2.6636(7)
	2.6667(11)		2.6678(7)
	2.6689(11)		2.7108(7)
	2.6689(12)		2.6436(7)
	2.6884(10)		2.6776(7)
	2.6892(11)		2.7186(7)
	2.6896(11)		2.6499(7)
	2.6959(12)		2.6567(7)
	2.6999(11)		2.7112(7)
mean	*2.6748(12)*	*2.6766(9)*	*2.6777(7)*
standard-deviation	*0.017*	*0.017*	*0.040*
***Cu-P** (Å)*	*2.244(2)*	2.250(2)*3	2.255(1)
	2.246(2)	2.264(3)	2.254(1)
	2.249(2)		2.261(1)
	2.255(2)		2.258(1)
mean	*2.249(2)*	*2.254(3)*	*2.257(1)*
standard-deviation	*0.005*	*0.007*	*0.003*
***I-Cu-I** (°)*	*102.81(4)*	106.70(3)*3	112.65(2)
	102.91(4)	106.78(3)*3	108.44(2)
	103.67(4)	109.74(3)*3	106.49(2)
	104.05(4)	110.41(3)*3	111.22(2)
	107.73(4)		107.08(2)
	108.40(4)		105.79(2)
	108.48(4)		108.82(2)
	108.81(4)		108.62(2)
	108.98(4)		106.37(2)
	110.93(4)		109.83(2)
	112.39(4)		108.97(2)
	112.92(4)		111.64(2)
mean	*107.67(4)*	*108.41(3)*	*108.83(2)*
standard-deviation	*3.568*	*1.759*	*2.200*

The three clusters were analyzed by solid-state NMR. The ^{13}C CPMAS NMR spectra are all similar with signals corresponding to the phenyl groups of the ligands (Figure S3). The solvent (hexane) in the crystalline structure of **2-CF$_3$** is also observed. The ^{31}P MAS spectra of the 3 compounds are shown in Figure 3. Because of the one-bond *J*-couplings between the ^{31}P nucleus and the copper isotopes of both nuclear spin value of 3/2 (^{65}Cu and ^{63}Cu with 30.9 and 69.1 % natural abundance, respectively), the signal of each phosphorus site consists in a multiplet composed of two overlapping quartets.[54] Therefore, the spectra of **C-CF$_3$** are all multiplets lying in the same chemical shift range. Comparatively, the lines of the **1-CF$_3$** and **2-CF$_3$** spectra are much broader than those of **3-CF$_3$** that reflects the presence of disorder of the ligands in the structure of two formers, as identified by SCXRD analysis.

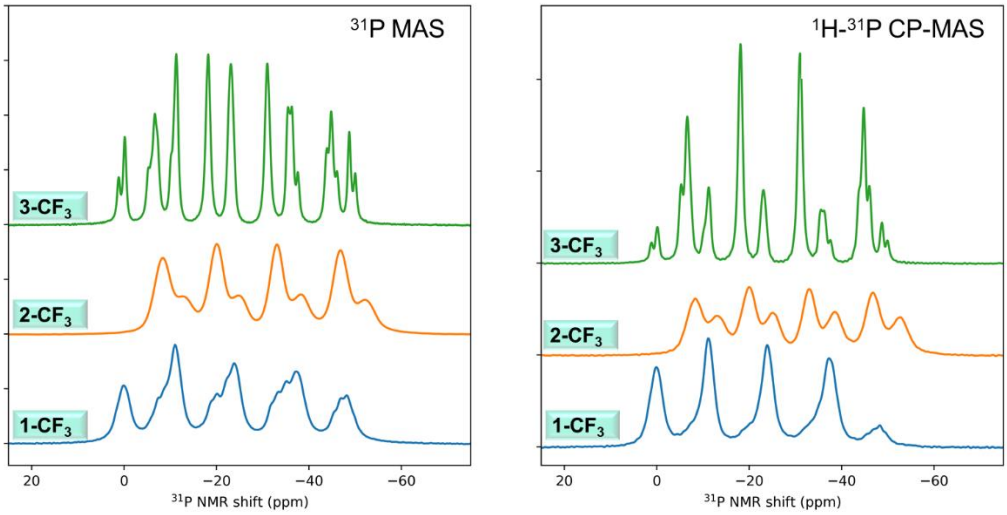

Figure 3. Solid-state ^{31}P MAS and ^{1}H-^{31}P CP-MAS NMR spectra of **C-CF$_3$**.

The ^{1}H-^{31}P CP-MAS spectra were also recorded and are shown in Figure 3. When comparing ^{31}P MAS and ^{1}H-^{31}P CP-MAS spectra, changes in the relative intensity of the peaks are observed for each of the three clusters. This effect is due to differences in the ^{1}H environments of the phosphorus sites in the ligands bearing the different C_6H_5 and C_6H_4-CF_3 groups. Linear combinations of the MAS and CP-MAS spectra allow the construction of two sub-spectra, as reported in Figure S4. For **1-CF$_3$**, each subspectrum accounts for half of the full signal corresponding to two of the four inequivalent phosphorus sites in the crystalline structure. The two associated isotropic chemical shifts can be estimated to -19 and -28 ppm. For **2-CF$_3$**, the first subspectrum accounts for one quarter of the full signal while the second corresponds to three quarters, in full agreement with the trigonal symmetry with two inequivalent P sites of 1:3 ratio. The estimated two associated isotropic chemical shifts are -28 and -34 ppm. Finally, for **3-CF$_3$**, each subspectrum accounts for half of the full signal *i.e.* two of the four non-equivalent phosphorus sites of the crystalline structure, as in **1-CF$_3$**. The isotropic chemical shifts of the two phosphorus sites associated with the first subspectrum are similar and close to -26 ppm. In opposite, for the second subspectrum, the isotropic chemical shifts of the two phosphorus sites are found different, around -18 and -32 ppm. Although, the increase of the electron withdrawing effect along the **1-3-CF$_3$** series is not clearly observed in the ^{31}P signal chemical shift values, these last are all in the range of values reported for copper iodide cubane clusters coordinated by phosphine ligands.[55–57]

The FTIR and Raman spectra of the **C-CF$_3$** clusters are reported in Figures 4 and 5. Simulations of the spectra were carried out by DFT calculations and the relatively good match with the experimental data permit to suggest an assignment of the vibrational bands (details in SI and Figures S5-6). FTIR spectra in the far-IR (50-650 cm^{-1}) and mid-IR (400-4000 cm^{-1}) regions are presented in Figure 4. Above 200 cm^{-1}, the three spectra are very similar and the bands can be all attributed to ligand vibrations. In particular, the C-H of the phenyl groups are found around 3050 cm^{-1}. Vibrations involving the CF_3 groups are also identified. The intense vibration at 1320 cm^{-1} can be attributed to the CF_3 antisymmetric stretching. In the 1200-1000 cm^{-1} range, the multiple peaks are from C-F stretching. The bands at 597 and 524 cm^{-1} can be attributed to CF_3 deformation modes. The vibrations of the [Cu_4I_4] inorganic core are found in the low frequencies region. In particular, two bands at around 90 and 130 cm^{-1} can be identified. While those of **1-CF$_3$** and **2-CF$_3$** have almost same position, those of **3-CF$_3$** are broader and shifted. These bands can be attributed to Cu-I vibrations (wagging and stretching) together with some [Cu_4I_4] core breathing motion, in accordance with the DFT simulations and previous studies.[58–61] These two low frequency bands appear to be a specific signature of the [Cu_4I_4] cubane moiety.

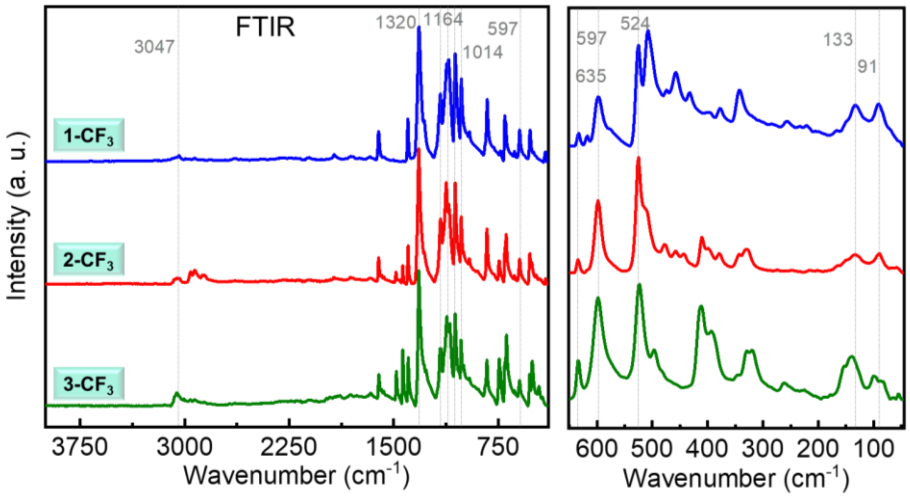

Figure 4. Far- and mid-FTIR spectra of **C-CF$_3$**.

Raman spectra from 65 to 3300 cm^{-1} are shown in Figure 5. The three spectra present similar signature and as for the FTIR analysis, vibrations above 200 cm^{-1} are from the ligands. The intense bands centered around 3060 cm^{-1} correspond to the C-H bond stretching of the phenyl groups. In accordance to the FTIR analysis, vibrations involving the CF_3 groups are observed. The band at 1327 cm^{-1} can be attributed to the carbon bearing the CF_3 moieties in a stretching motion with the carbon of the phenyl group. Between 1000 and 1102 cm^{-1}, four intense bands are observed for **1-CF$_3$** and **2-CF$_3$**, whereas two are only present for **3-CF$_3$** which is also nicely reproduced by the simulations (Figure S6). The one at 1063 cm^{-1} is assigned to C-F stretching and the three others are from the phenyl groups. In particular, the two bands at 1000 and 1030 cm^{-1} can be attributed to the unsubstituted phenyl group (C_6H_5) only present in **1-CF$_3$** and **2-CF$_3$**, in opposite to the substituted one centred at 1102 cm^{-1} (C_6H_4-CF_3) present in the three clusters. Similarly, the band at 1610 cm^{-1} correspond to C-C stretching of the substituted phenyl group whereas that at 1588 cm^{-1} is from the unsubstituted one. The band at 525 cm^{-1} is attributed to CF_3 deformation modes and the one at 781 cm^{-1} to C-C stretching modes of the phenyls. Broad bands are observed at low frequency which can be assigned to vibrations of the [Cu_4I_4] cluster core. In

particular those found around 80, 115 and 150 cm^{-1} correspond to Cu-Cu and Cu-I movements, in agreement with previous studies[58–61] and simulations.

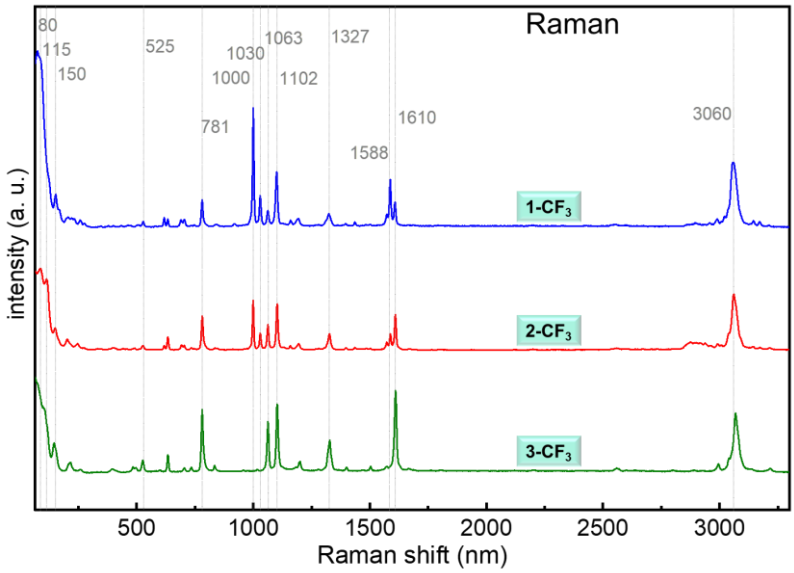

Figure 5. Raman spectra of **C-CF₃**.

2.2. Photoluminescence properties.

The crystalline powders of **C-CF₃** are white under ambient light and display photoluminescence properties under UV light. While **3-CF₃** presents a blue emission, **1-CF₃** emits a white color whereas **2-CF₃** displays an intermediate whitish emission, at room temperature (Figure 6). When the powders are cooled to liquid nitrogen temperature, their emission all change to blue with a deeper blue color for **3-CF₃**. Upon warming up to room temperature, the pristine emissions are recovered, indicating a completely reversible thermochromic luminescence properties for the **C-CF₃** clusters series.

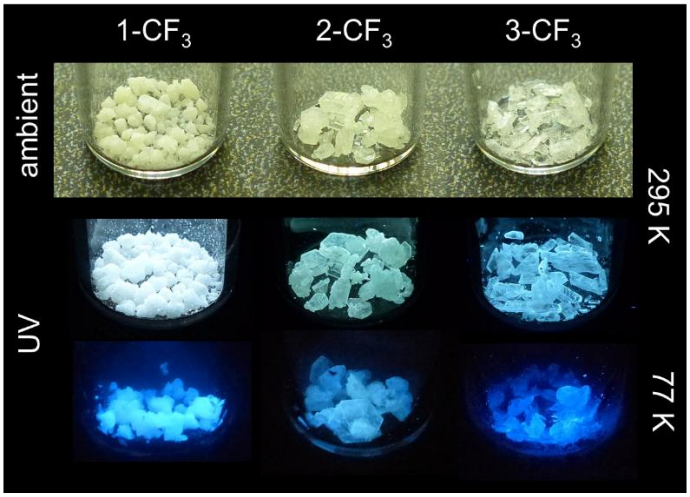

Figure 6. Photos of the crystalline powders of **C-CF₃** under ambient light and under UV (365 nm lamp) at room temperature (295 K) and in liquid nitrogen (77 K).

Solid-state emission and excitation spectra of the clusters from 295 to 77 K are shown in Figure 7. The corresponding data are reported in Table 2. At 295 K, the emission spectra present two unstructured emission bands, one in the blue and the other in the yellow region, namely HE (High Energy) and LE

(Low Energy), respectively. These bands are centered at 450 and 560 nm for **1-CF$_3$**, at 445 and 550 nm for **2-CF$_3$** and at 445 and 520 nm for **3-CF$_3$** (λ_{ex} = 350 nm). The intensity of the yellow LE band increases comparatively to that of the blue HE one as of the number of CF_3 groups decreases, from **3** to **1-CF$_3$** cluster. The different relative intensities of these two bands are therefore in agreement with the emission color observed by the naked eyes with the bluer emission displayed by **3-CF$_3$** and the whitish and white emission by increasing the yellow contribution, for **2-CF$_3$** and **1-CF$_3$**, respectively. The CIE chromaticity coordinates clearly illustrate the effect of the number of CF_3 groups with values of (0.34; 0.40), (0.31; 0.37) and (0.23; 0.28) for **1-3-CF$_3$** respectively, with the first two close to pure white emission (0.33; 0.33). The PLQY (absolute internal quantum yields) measured at room temperature are 41, 33 and 6 % for **1-3-CF$_3$** respectively, (λ_{ex} = 350 nm, Table 2). The lower value of **3-CF$_3$** may be attributed to more important non-radiation processes because of its more flexible structure due to its higher number of CF_3 groups. Emission lifetimes were recorded for the two HE and LE emission bands of each cluster, at 295 K. The emissions all present biexponential decay with values in the microsecond range (Table 2), as commonly observed for these phosphorescent clusters.[42,45,51,55,62] A shorter component is systematically observed for the HE emission compared to the LE one, in accordance to previous reports.[42,45,51]

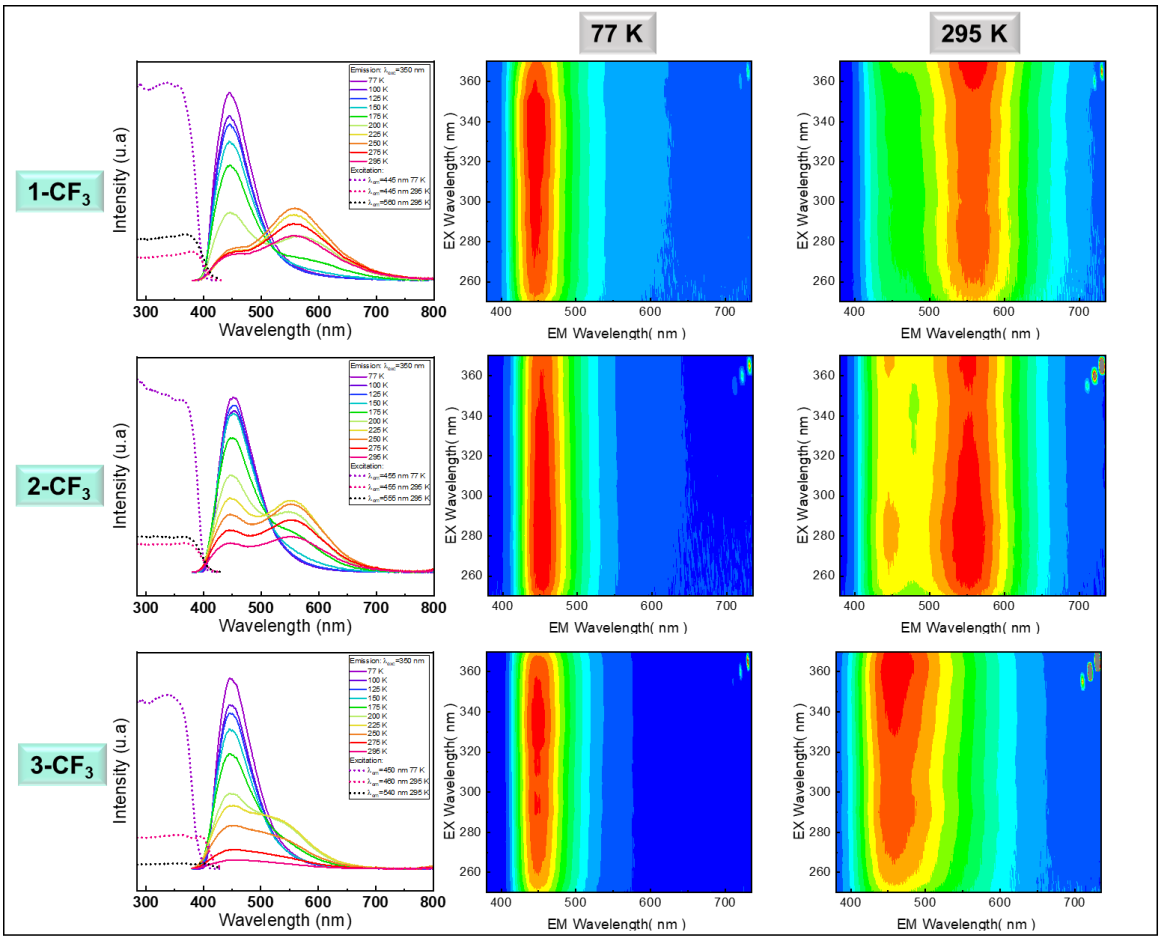

Figure 7. Temperature-dependent solid-state luminescence spectra of **C-CF$_3$** with emission in solid and excitation spectra in dashed or dotted lines, and excitation (250-370 nm) *vs* emission (380-735 nm) cartographies (λ_{ex} *vs*. λ_{em}) at 77 and 295 K.

Upon lowering the temperature, the relative intensity of the two emission bands varies with a similar behavior for the three clusters. In the 295-200 K range, the intensity of the LE band increases comparatively to the HE one. Below 200 K, the intensity of the LE band decreases progressively. At 77 K, the LE band has disappeared and the HE band becomes the only one observed, leading to the blue emission observed by the naked eyes (Figure 6). Accordingly, the CIE coordinates at 77 K are (0.16; 0.12), (0.16; 0.14) and (0.15; 0.12) for **1-3-CF$_3$**, respectively. The intensity increase of the LE band followed by its decrease upon cooling, can be explained by first, the classical enhancement of radiative processes and then, by excitation competition with the HE related excited state. The excitation profiles of the two emission bands are almost similar for the three clusters. From the excitation *vs* emission cartographies (Figure 7), both the HE and LE bands can be excited in a large 250-370 nm wavelength range at 77 and 295 K. Excitation-dependent emission is also displayed by the **C-CF$_3$** clusters and in particular at room temperature for which the relative intensity of the LE and HE bands can vary. The Stokes shift between excitation and emission maxima of the LE bands of 1.33, 1.29 and 1.16 eV for **1-3-CF$_3$** respectively, are as expected, much larger compared to those of the HE bands of 0.79, 0.76 and 0.76 eV, respectively.

Table 2. Photoluminescence data of **C-CF$_3$** clusters recorded at λ_{ex}=350 nm. Lifetimes (τ) recorded at λ_{ex}=340 nm and 295 K with amplitude percentages in brackets. Photoluminescence quantum yields (PLQY) recorded at 295 K.

	λ^{max}_{em}] 77 K		λ^{max}_{em} 200 K		λ^{max}_{em} 295 K		τ (μs) [λ_{ex} = 340 nm]	PLQY (%) [λ_{ex} = 350 nm]
	HE	LE	HE	LE	HE	LE		
1	450	-	445	565	450	560	2.0 (36 %) 5.7 (64 %) [HE] 4.3 (55 %) 6.6 (45 %) [LE]	41
2	450	-	450	550	445	550	1.6 (39 %) 4.0 (61 %) [HE] 7.7 (3 %) 22.9 (97 %) [LE]	33
3	445	-	450	520	445	520	1.6 (97 %) 6.0 (3 %) [HE] 1.7 (97 %) 8.5 (3 %) [LE]	6

DFT calculations were conducted to rationalize the luminescence properties of the **C-CF$_3$** clusters series. The geometries of the singlet ground states (S_0) were optimized (see computational details in SI). Unfortunately, all our attempts to relax any of the lowest triplet states failed. Relevant computed data of the cluster's geometry at S_0 are reported in Table 3 along with corresponding SCXRD data (in brackets). The computed values in D_2 and *T* symmetries for **1-2-CF$_3$** and **3-CF$_3$** respectively, are in a satisfying agreement with the experimental ones, as illustrated for the Cu-Cu distances (Figure S7).

Table 3. Geometrical parameters (mean values) of the optimized DFT structures at the ground state (S_0) of **C-CF$_3$** compared with the SCXRD data in brackets.

	1-CF$_3$	**2-CF$_3$**	**3-CF$_3$**
	S_0 (D_2)	S_0 (D_2)	S_0 (T)
HOMO-LUMO gap (eV)	4.24	4.18	4.22
Cu-Cu (Å)	3.088 [3.015(1)]	3.008 [2.979(1)]	3.002 [2.953(1)]
Cu-I (Å)	2.715 [2.675(1)]	2.711 [2.677(1)]	2.715 [2.678(1)]
Cu-P (Å)	2.347 [2.249(2)]	2.308 [2.254(3)]	2.346 [2.257(1)]

The ground state electronic structures of the **C-CF$_3$** clusters were calculated and their Kohn-Sham orbital diagrams are presented in Figure 8. The HOMO-LUMO band gaps values (4.24, 4.18, 4.22 eV for **1-3-CF$_3$**, respectively) are close in energy, fully explaining that the observed experimental optical properties remain in the same energies range. The HOMOs (Highest Occupied Molecular Orbitals) are mainly composed of copper (3d) and iodine (5p) orbitals (34, 35 % and 43 % respectively, for all clusters). The 24 lowest unoccupied orbitals (LUMO-LUMO+23) form a block of orbitals which are combinations of the π* orbitals of the phenyl groups of the phosphine ligands. Just above this block of 24 orbitals lies an in-phase orbital of *a* symmetry (LUMO+24) of large Cu 4s/4p character (80 %), for the three clusters.

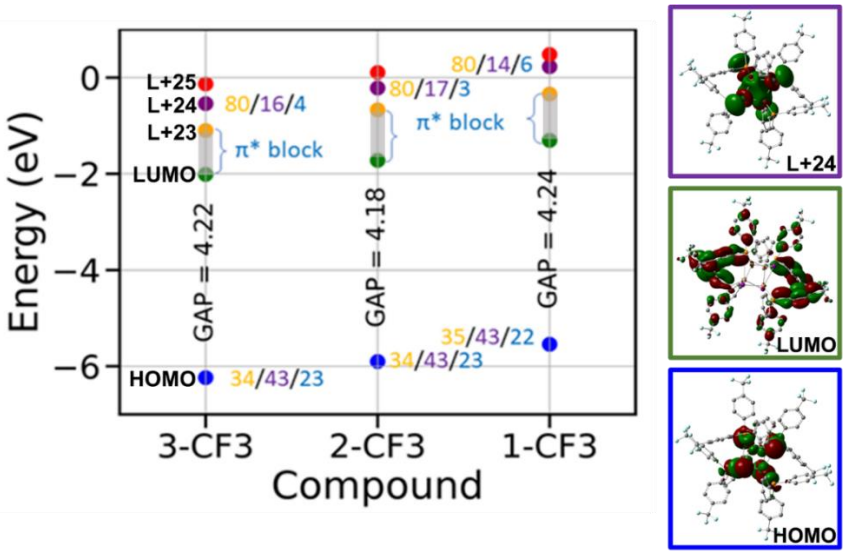

Figure 8. Kohn-Sham orbital diagram of **C-CF$_3$** at the ground state (S_0). The MO localizations (in %) are given in the following order: Cu/I/P. Orbital plots of the HOMO, LUMO and LUMO+24 of **2-CF$_3$** with Cu atoms in orange, I in purple, F in blue, and the others in grey.

The electronic transitions of lowest energy have been calculated by TD-DFT (Time Dependent-DFT). The calculated absorption transitions correspond to electron promotion from the HOMO to one of the lowest π* combination localized on the ligands. Such transitions are thus of mixed ^{1}(X+M)LCT character (X and M for I and Cu, respectively). The calculated spectra show broad bands in the 310-320 nm range and centred around 350 nm (Figure S8). This result is in fair agreement with the experimental UV-visible spectra of **C-CF$_3$** exhibiting broad absorption bands around 280 and 340 nm (Figure S9).

Based on previous studies on **C3-CF$_3$** and other cubane copper iodide clusters, the emission properties of the clusters can be rationalized as follows.[48,59,63] The HE emission band has for origin the promotion of an electron from the HOMO into one of the LUMO-LUMO+23 orbitals which generates the T_2 excited state corresponding to a ^{3}(X+M)LCT transition. Regarding the LE emission, the electron goes to the LUMO+24 orbital having a strong Cu character. Due to its nature, this transition is named ^{3}CC for Cluster Centered (XMCT+MM), and causes a substantial shortening of the Cu-Cu distances which significantly stabilizes this other T_1 triplet state compared with the T_2 one. The luminescence thermochromism can be thus interpreted by the thermal equilibrium between these two T_2 and T_1 states.

T_2 is populated at low temperature leading to the HE emission. As temperature rises, the energy barrier is overpassed and T_1 is populated from T_2 and the LE emission occurs, as schematized in the simplified energy diagram in Figure 9. Temperature variation of the relative intensity of the HE and LE emission bands thus leads to the displayed thermochromism.

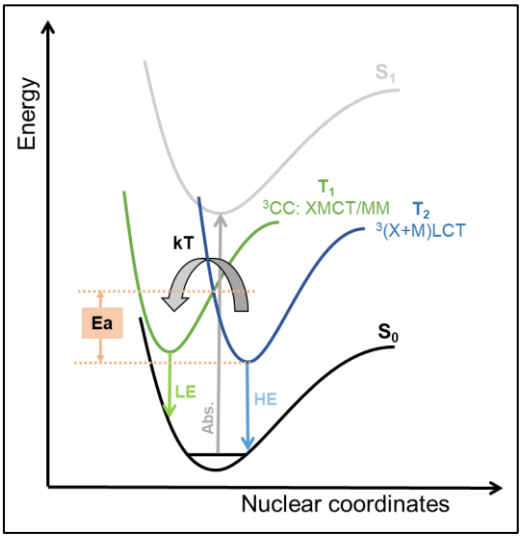

Figure 9. Simplified energy diagram illustrating the thermal equilibrium between the two excited states of **C-CF$_3$**.

By analysing the **C-CF$_3$** series, the effect of the electron withdrawing properties of the CF_3 groups of the ligands appears as energy stabilization of the whole orbitals' layout (Figure 8). The energy of the orbitals thus decreases from **C1-CF$_3$** to **C3-CF$_3$** by roughly 0.7 eV, while the band gaps values are almost constant for the three clusters. This agrees with the similar energy of the absorption bands and of the HE emission (450 nm at 295 K) of the three clusters. Interestingly, the energy difference between the LUMO and the LUMO+24 increases significantly from **1-CF$_3$** to **3-CF$_3$** with values of 1.534, 1.504 and 1.471 eV, respectively. This energy difference can be related to the energetic barrier to overcome to excite the T_1 state from the T_2 one (Figure 9). Therefore, as the LUMO+24 is getting less accessible, the excitation of the T_1 state is less probable and so the LE emission. This agrees with the different relative intensity of the LE and HE emission bands of the three clusters. Indeed, as the number of CF_3 groups decreases, the intensity of the LE band increases going from **3-CF$_3$** to **1-CF$_3$**, that is fully in accordance to our expectations. While **1-CF$_3$** and **2-CF$_3$** presents similar LE emission wavelengths (560 and 550 nm at 295 K, respectively), that of **3-CF$_3$** is blue shifted (520 nm at 295 K). The energy of this transition is commonly reported to be dependent on the Cu-Cu interactions due to the copper bonding nature of the ^{3}CC excited state.[59,63–65] Here, no correlation can be established because the Cu-Cu distances are almost similar in the three clusters (SCXRD Table 1). Other phenomenon must be involved in this de-excitation pathway, typically in the non-radiative molecular distortion relaxation.

2.3. Luminescence thermometry.

In order to get samples suitable for applications, composite materials were synthesized by incorporating the **C-CF$_3$** clusters within a polymer matrix. PMMA (polymethylmethacrylate) polymer was chosen for its good chemical stability and transparency in the UV-visible region. Clusters and PMMA were mixed in solution, dichloromethane was used but other solvents could also be employed. After evaporation of

the solvent, bulk and film samples were obtained whose shape can be easily varied depending on the mold used. The composite materials thus obtained, namely **Px-CF$_3$** (P for polymer, and x = 1 to 3), were colorless and crack-free (Figure 10). Due to the very good dispersion of the cluster within the polymer matrix, the composites are transparent up to 40 wt.% of cluster. Beyond this value, the composites become white and diffusive. The preservation of the clusters within the composites was attested by Raman spectroscopy. The main vibrational bands of the clusters are indeed observed in the spectra of the composites which are absent in the pure PMMA polymer (Figure S10). As shown in Figure 10, all the three **P-CF$_3$** composites are photoluminescent under UV irradiation with emission color ranging from white to blue, in accordance to the cluster's emission properties.

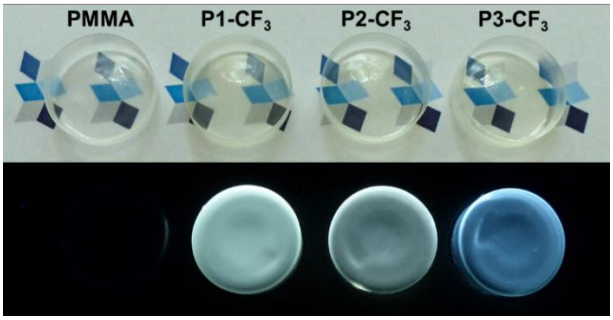

Figure 10. Photos of the composite materials **Px-CF$_3$** (x = 1-3, 10 wt.%) as pellets under ambient light (top) and under UV (bottom, 365 nm lamp) at room temperature (295 K).

Solid-state emission and excitation spectra of the **P-CF$_3$** composites from 77 to 315 K are shown in Figure 11a and the corresponding data are reported in Table S2. Similarly to the corresponding clusters, the emission spectra present two unstructured emission bands, one blue (HE) and the other yellow (LE), whose relative intensities vary for the different **C-CF$_3$** clusters. The two bands are centered at 460 and 545 nm for **P1-CF$_3$** (λ_{ex} = 350 nm), at 460 and 550 nm for **P2-CF$_3$** (λ_{ex} = 345 nm) and at 445 and 540 nm for **P3-CF$_3$** (λ_{ex} = 350 nm). The different relative intensities of the two bands lead to white to blue emission color of the composites whose CIE coordinates are (0.27; 0.31), (0.28; 0.31) and (0.22; 0.23) for **P1-3-CF$_3$**, respectively (Figure 11b). From the excitation *vs* emission cartographies (Figure S11), the HE presents a larger excitation wavelength range compared to the LE one at 295 K. This indicates a more pronounced excitation-dependent emission for the **P-CF$_3$** materials compared with the powders, leading to possible emission color tuning. The Stokes shifts for the LE bands of 1.27, 1.29 and 1.25 eV, are again larger compared to those of the HE bands of 0.85, 0.85 and 0.76 eV, for **P1-3-CF$_3$**, respectively. The PLQY measured at 295 K of 27, 29 and 23 % for **P1-3-CF$_3$** respectively, (λ_{ex} = 350 nm, Table S2) are relatively high values, relevant for application perspectives. Emission lifetimes for the two HE and LE emission bands all present triexponential decay with values in the microsecond range (Table S2), as for the powders. However, a longer component is observed around 10 µs for the composites. This result and the relatively similar PLQY values may imply a somehow protective effect of the polymer matrix with less nonradiative phenomena of the incorporated clusters. When lowering the temperature to 77 K, the **P-CF$_3$** exhibit a similar thermochromic behavior than the clusters with a decrease of the LE emission and concomitant increase of the HE one (Figure 11a and Figure S11). The opposite intensity variation of the HE and LE emission bands with temperature, as illustrated by the temperature-dependent integrated intensity (A) of the two bands (A_{HE} and A_{LE} in Figure 11c), renders the composites appealing as ratiometric luminescent thermometers.

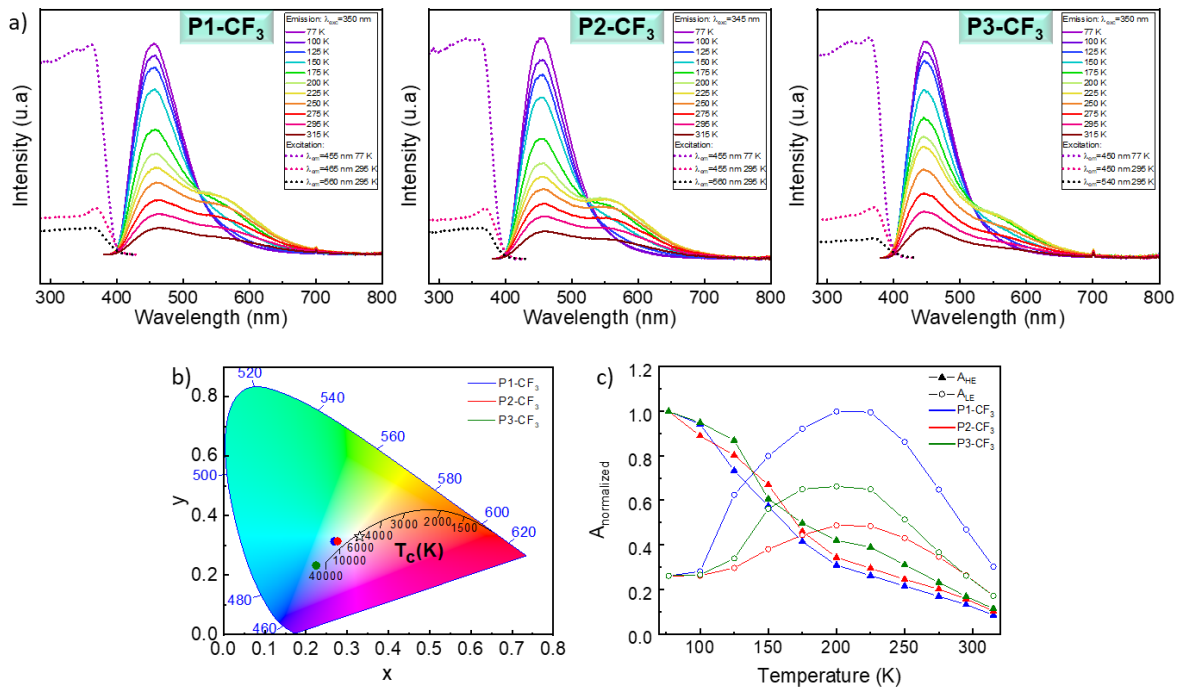

Figure 11. (a) Temperature-dependent solid-state luminescence spectra of **P-CF₃** with emission in solid and excitation spectra in dotted lines between 77 and 315 K. (b) CIE chromaticity coordinates diagram (1931). (c) Thermal evolution of the integrated intensity of the HE and LE bands, A_{HE} and A_{LE} (determined by Gaussian decomposition).

To evaluate the thermometric performances of **P-CF₃** composites, the $\Delta = A_{HE}/A_{LE}$ intensity ratio was determined and due to the overlap of the two emission bands two different approaches were studied and compared. The first approach we used is the most common way consisting in integrating the area of the emission band limited by two arbitrary chosen zones: 390-512 nm for A_{HE} and 512-690 nm for A_{LE} (Figure S12a). The second approach is the fit of the emission spectrum using Gaussian curves to get the whole integrated area of each band (Figure S12b). Although this latter way was highlighted by Brites *et al.*[66] on upconverting Y_2O_3:Yb^{3+}/Ho^{3+}/Tm^{3+} nanocrystals, it is not widespread in the community, and has never been applied to copper(I) compounds.[67–72] For both approaches, the thermal evolution of the thermometric parameter $\Delta = A_{HE}/A_{LE}$ was plot, and fit with the Boltzmann function from Origin® software (Figure S13), all fitting parameters being reported in Table S3.

In order to evaluate the thermal performances of **P-CF₃**, we then calculated the relative thermal sensitivity defined as $S_r = |\partial\Delta/\partial T|/\Delta$ which is a usual figure of merit to compare the performances of distinct ratiometric systems (Figure 12). First, by comparing the two approaches to determine the integrated emission intensity, we can see that integrating two different zones of emission spectrum underestimates the relative thermal sensitivity (Figure 12, Table 4), as also reported by Brites *et al.*.[66] Thus, with this approach the most performant composite is **P2-CF₃** with a maximum of relative thermal sensitivity (S_m) of 2.27 $\%K^{-1}$ while **P1-CF₃** reaches a S_m value of 3.73 $\%K^{-1}$ with the Gaussian fit. Consequently, the use of Gaussian decomposition seems more appropriate when an important overlap between emission bands exists. If the thermal sensitivities are similar for **P1** and **P3-CF₃**, **P2-CF₃** appears less sensitive (S_m = 2.83 $\%K^{-1}$) probably due to the presence of solvent molecules in the structure which can act as quenchers. The thermal evolution of A_{HE} and A_{LE} (Figure 11c) shows that the thermal

quenching of the HE emission band is superimposable for all composites while the increase of the LE emission depends on the number of CF_3 groups of the ligand. Thus, the largest variation appears for **P1-CF$_3$** while the lowest one concerns **P2-CF$_3$**. We can therefore establish a correlation between the highest thermal sensitivity and the most pronounced opposite trend in the temperature dependency of the emissions, *i.e.* for **P1-CF$_3$**, in line with the report by Cheng *et al.*.[73]

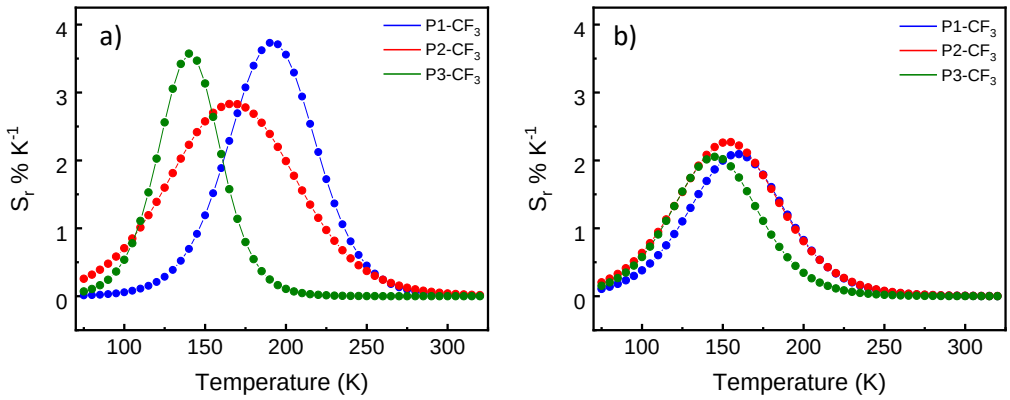

Figure 12. Relative thermal sensitivity (S_r) in the 77-315 K temperature range for **P-CF$_3$** composites a) for integrated areas A_{HE} and A_{LE} obtained from Gaussian decomposition, and b) for integrated areas A_{HE} and A_{LE} obtained with arbitrary interval integration.

For comparison, analogue investigation was conducted for **C-CF$_3$** clusters, and similarly higher relative thermal sensitivities with the Gaussian decomposition were obtained (Figure S14-S15, and Table S4). Noticeably, the **C-CF$_3$** clusters are more sensitive than the **P-CF$_3$** composites for which lower intensity of the LE band is probably due to less rigid environment in the polymer reducing radiative phenomena. Furthermore, comparison along the **C-CF$_3$** series reveals that, this time, the **3-CF$_3$** cluster is the most performant material with a S_m value at 4.87 $\%K^{-1}$. Finally, all materials present relatively high values of thermal sensitivities compared to other reported systems,[66–72] which lie in the medium temperature range, *i.e.* between 100 and 300 K. Note that the T_m value, *i.e.* the temperature where the relative sensitivity is maximum, shifts from 140 to 190 K when the number of CF_3 groups of the ligand decreases (Table 4). This may be related to the energy gap between the HE and LE excited states, which depends on the withdrawing effect of the CF_3 groups (Figure 9).

Table 4. Maximum relative thermal sensitivity (S_m) and temperature at maximum sensitivity (T_m) of **C-CF$_3$** and **P-CF$_3$** obtained from both approaches. Gauss is for integrated intensities obtained by Gaussian decomposition and int by arbitrary interval integration.

	C-CF$_3$			**P-CF$_3$**		
	1	**2**	**3**	**P1**	**P2**	**P3**
$S_{m\ gauss}$ ($\%K^{-1}$)	4.15	3.73	4.87	3.73	2.83	3.57
$S_{m\ int}$ ($\%K^{-1}$)	3.80	3.33	3.63	2.09	2.27	2.05
$T_{m\ gauss}$ (K)	210	190	170	190	165	140
$T_{m\ int}$ (K)	190	180	175	160	155	145

To evaluate whether the material could be used as a reliable thermometer, cycle tests were additionally performed on **P1-CF$_3$**, and the repeatability was calculated according the equation (1):

$$R = 1 - \frac{max|\Delta_c - \Delta_i|}{\Delta_c} \qquad (1)$$

where Δ_C is the mean thermometric parameter, and Δ_i is the value of each measurement of the thermometric parameter. Then, four cycles between 150 and 200 K were carried out (Figure S16) to get a repeatability R > 97 %, which confirms the robustness of the **P-CF₃** materials for an application as luminescent thermometers.

2.4. Solid-state lightening: pc-w LED.

Owing to the relevant properties of the **C-CF₃** clusters as white emitters and their large Stokes shift, they were further studied as single-component phosphors for energy-efficient solid-state lightening. The composite materials were then employed as converting layers to fabricate pc-wLEDs. Taking advantage of the processability of the **P-CF₃** composites, they were coated onto commercially available 365 nm GaN chips. Photos of the operating LEDs devices, of the luminescence spectra and corresponding CIE diagrams, are gathered in Figure 13.

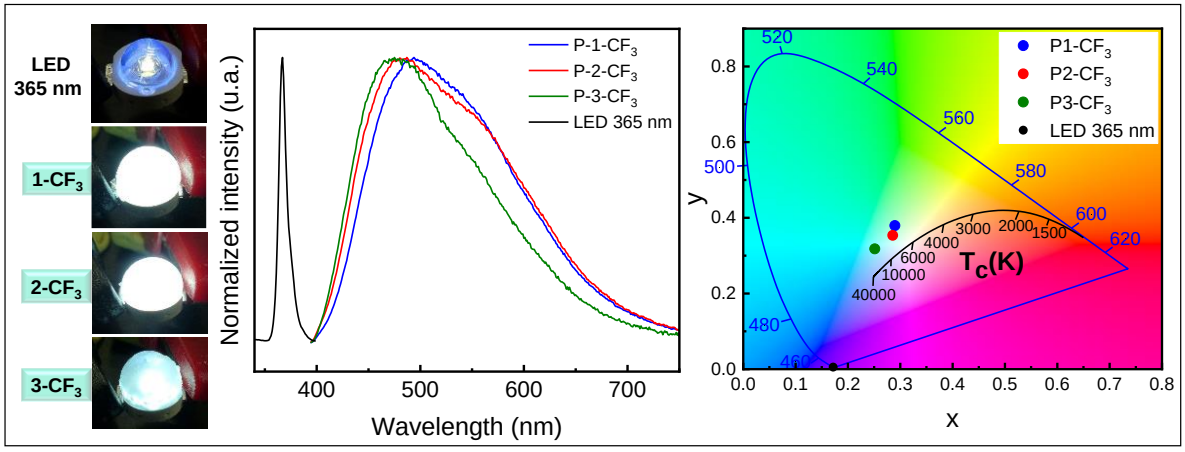

Figure 13. Photos of the 365 nm-LEDs coated with **P-CF₃** materials (cluster content 30 wt.%), corresponding emission spectra and CIE diagram coordinates, at room temperature (295 K).

The emission spectra present the broad emission band of the compounds ranging from 400 to 750 nm. Differences with the **P-CF₃** properties, in particular the intensity of the LE emission band, is ascribed to the different excitation wavelength of the LED. The corresponding CIE chromaticity coordinates of the LEDs are (0.29; 0.38), (0.29; 0.35), (0.25; 0.32) for **1-3-CF₃** respectively. While **P3-CF₃** LED lies in the blue region, the first two are close to pure white light (0.3, 0.3), in accordance to the emitting white light observed (Figure 13). The light emitting devices exhibit color temperature (CCT) of 7154, 7667 and 11319 K and color rendering index (CRI) of 73, 78 and 75 for **1-3-CF₃** respectively, which are relevant for quality white light for indoor lighting applications. While most examples of white emissive phosphor-converted LED based on copper iodide complexes are reported by employing two or more additional emitters (commercial), the present results demonstrate that the studied copper iodide clusters are relevant as a single-component emitting phosphors for PC-wLED lighting applications.

2.5. Multifunctional luminescent inks: anticounterfeiting

The distinguishable emission features of the **P-CF₃** composite materials exhibiting temperature and excitation-dependent emission and their excellent ink-forming ability, prompt us to investigate their anticounterfeiting applications. Inks of the three clusters were synthesized by dissolving **C-CF₃** (10 wt.%) in a solution of PMMA in ethyl acetate. As displayed in Figure 14, a landscape could be

drawn on filter paper, by filling a pen with the different inks. To make the landscape sunnier, a yellow emissive ink was additionally used by employing a yellow phosphor. The latter is also a cubane copper iodide cluster formulated $[Cu_4I_4L_4]$ L = $PPh_2(CH_2CH_2CH_3)$, known for its intense yellow emission and thermochromic properties.[74]

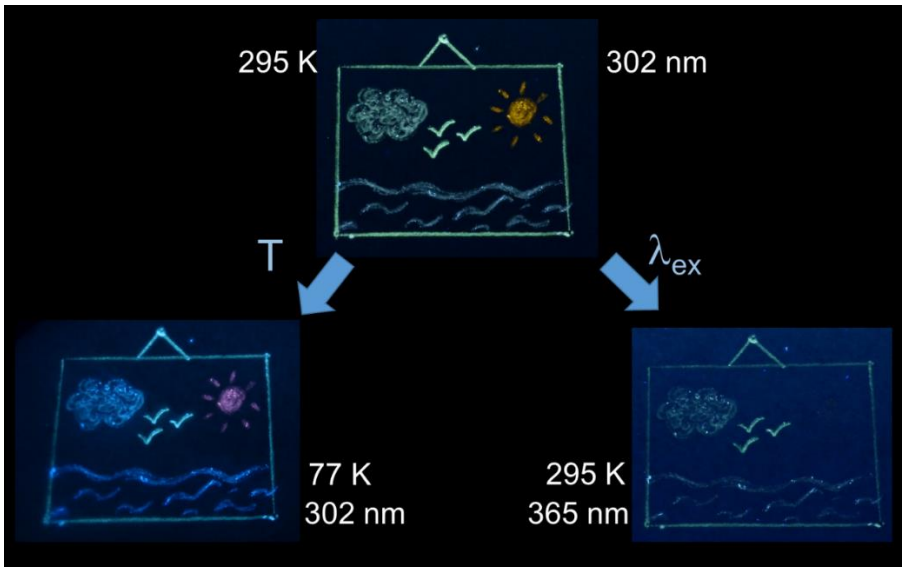

Figure 14. Photos of a landscape painted by using **C-CF3** as inks, at different temperature (295 and 77 K) and under different excitation lamp (302 and 365 nm).

While invisible in natural light due to the colorless inks, the landscape displays under UV irradiation, the four-emission color pattern of the clusters of blue, green white to yellow light. The temperature- and excitation-dependent emission of the compounds offer additional protection for multi-mode anticounterfeiting applications. Therefore, at low temperature a change of the color of the drawing in the blue region, is clearly visualized, in accordance to the luminescent thermochromic properties of the clusters (77 K in Figure 14). Similarly, by changing the excitation wavelength (365 nm in Figure 14), the emission color become greener and disappearance of the sun even occurs. This result demonstrates the anti-counterfeiting application prospects of the studied copper iodide clusters thanks to their specific luminescence and processability of characteristics, which can also be relevant for information encryption and transmission.

3. Conclusion.

The rational design of copper iodide clusters for developing single-component white-light emitters by ligand engineering, is described in this study. Original single-component white-emissive copper iodide clusters are thus reported that expand the library of cost-effective copper-based white emitters. By synthetic adjusting the electron withdrawing character of the phosphine ligands, the energy layout of the molecular clusters could be tuned to get dual emission feature in the visible range, appropriate for white emission. The compounds were structurally characterized by X-ray diffraction, solid-state NMR and vibrational spectroscopies. DFT calculations permit to rationalize the effect of the ligand on the photophysical properties of the clusters. Modification of the interplay between the two triplet states appears to be responsible for the different relative intensity of the two emission bands. The white

emissive clusters present intense photoluminescence and high-contrast thermochromic properties with temperature-dependent intensity variation of the dual emission feature. The good solubility of the studied compounds in a wide range of solvents, permit the synthesis of composite materials by incorporation into a polymer matrix. The processability of these polymer materials allowed us to study of their potential applications in diverse fields.

The luminescence thermochromism displayed by the clusters appears perfectly adapted for luminescence thermometry applications. The study of their ratiometric thermometry properties revealed high relative thermal sensitivity values in the medium temperature range. These findings show that these compounds are highly promising candidates for luminescence thermometry applications based on ratiometric detection. Their use as single-component emitting phosphors for white LED lighting is also reported. The coating of a blue-LED with the composite materials permit to get phosphor-converted white-light emitting diodes without additional commercial phosphor. The measured color temperature and color rendering indexes are relevant for indoor lighting applications. The facile preparation, excellent solubility and ink-forming ability of the studied compounds combined with their switchable emission in response to excitation and temperature, also allowed us to evaluate their anticounterfeiting properties. Multicolor drawings could thus be realized that emission colors can be modified upon temperature and the emission wavelength changes. These results demonstrated the great potential of these phosphors in multi-mode anticounterfeiting applications.

Finally, aside significant perspectives of applications of the reported copper halide materials, this study emphasizes the power of ligand design strategy to achieve specific target properties that enable the development of advanced multifunctional materials based on cost-effective and eco-friendly light-emitting copper materials.

Supporting Information.

Supporting information is available from the Wiley Online Library or from the authors.

Acknowledgments.

The ‘Région Pays de la Loire’ and the Defense innovation Agency are thanked for financial support of the Ph.D. fellowship of A. Rocheteau. This work received financial support under the EUR LUMOMAT project. E. Ishow is gratefully acknowledged for lifetimes measurements. T. Roisnel is thanked for help in structures analyses. Luminescence, Raman, XRD and solid-state NMR were performed on IMN’s equipment platform, PLASSMAT, Nantes, France. C. Latouche is grateful for financial support from the Institut Universitaire de France (IUF). The CCIPL (Centre de Calculs Intensifs des Pays de Loire) is acknowledged for computational resources.

References.

[1] O. S. Wenger, *J. Am. Chem. Soc.* **2018**, *140*, 13522.
[2] B. Su, J. Jin, K. Han, Z. Xia, *Adv. Funct. Mater.* **2023**, *33*, 2210735.
[3] S. Li, J. Xu, Z. Li, Z. Zeng, W. Li, M. Cui, C. Qin, Y. Du, *Chem. Mater.* **2020**, *32*, 6525.
[4] Z. Xu, L. Jiang, H. Xiong, J. Wen, P. Li, L. Lin, B. Wu, A. Yang, Y. Qiu, *Chem. Commun.* **2023**, *59*, 5677.
[5] J. Qu, S. Xu, H. Shao, P. Xia, C. Lu, C. Wang, D. Ban, *J. Mater. Chem. C* **2023**, *11*, 6260.

[6] R. Hamze, J. L. Peltier, D. Sylvinson, M. Jung, J. Cardenas, R. Haiges, M. Soleilhavoup, R. Jazzar, P. I. Djurovich, G. Bertrand, M. E. Thompson, *Science* **2019**, *363*, 601.
[7] Z. Xiao, Z. Song, Y. Yan, *Advanced Materials* **2019**, *31*, 1803792.
[8] D. B. Straus, S. Guo, A. M. Abeykoon, R. J. Cava, *Advanced Materials* **2020**, *32*, 2001069.
[9] D. Banerjee, B. Saparov, *Chem. Mater.* **2023**, *35*, 3364.
[10] J.-S. Yao, J.-J. Wang, J.-N. Yang, H.-B. Yao, *Acc. Chem. Res.* **2021**, *54*, 441.
[11] X. Fan, F. Yuan, J. Wang, Z. Cheng, S. Xiang, H. Yang, Z. Zhang, *CCS Chemistry* **2022**, *5*, 350.
[12] D. Kim, M. C. Rosko, F. N. Castellano, T. G. Gray, T. S. Teets, *J. Am. Chem. Soc.* **2024**, *146*, 19193.
[13] S. Lin, Z. Ma, X. Ji, Q. Zhou, W. Chu, J. Zhang, Y. Liu, Y. Han, L. Lian, M. Jia, X. Chen, D. Wu, X. Li, Y. Zhang, C. Shan, Z. Shi, *Advanced Materials* **2024**, *36*, 2313570.
[14] R. Gu, K. Han, J. Jin, H. Zhang, Z. Xia, *Chem. Mater.* **2024**, *36*, 2963.
[15] Q. Hu, C. Zhang, X. Wu, G. Liang, L. Wang, X. Niu, Z. Wang, W.-D. Si, Y. Han, R. Huang, J. Xiao, D. Sun, *Angew. Chem. Int. Ed.* **2023**, *62*, e202217784.
[16] Y. Zhan, P. Cai, X. Pu, Q. Ai, J. Si, X. Yao, G. Bai, Z. Liu, *Inorg. Chem. Front.* **2024**, *11*, 579.
[17] W. Zhu, R. Li, X. Liu, X. Xu, H. Chao, H. Wang, Y. Jiao, H. Liu, F. Xu, Z. Nie, Y. Gao, R. Wang, J. Zhu, W. Huang, *Advanced Functional Materials* **2024**, *34*, 2316449.
[18] N. Lin, X. Wang, H.-Y. Zhang, K.-Q. Sun, L. Xiao, X.-Y. Zhang, C.-Y. Yue, L. Han, Z.-W. Chen, X.-W. Lei, *ACS Appl. Mater. Interfaces* **2024**, *16*, 41165.
[19] T.-Y. Li, S.-J. Zheng, P. I. Djurovich, M. E. Thompson, *Chem. Rev.* **2024**, *124*, 4332.
[20] J.-J. Wang, L.-Z. Feng, G. Shi, J.-N. Yang, Y.-D. Zhang, H. Xu, K.-H. Song, T. Chen, G. Zhang, X.-S. Zheng, F. Fan, Z. Xiao, H.-B. Yao, *Nat. Photon.* **2023**, 1.
[21] K. Chen, B. Chen, L. Xie, X. Li, X. Chen, N. Lv, K. Zheng, Z. Liu, H. Pi, Z. Lin, A. L. Rogach, *Adv. Funct. Mater.* **2024**, *34*, 2310561.
[22] X. Lu, S.-J. Wu, Y.-S. Wang, S.-Y. Wei, L. Meng, X.-H. Huang, X.-L. Chen, C.-Z. Lu, *Inorg. Chem. Front.* **2024**, *11*, 2775.
[23] W. Liu, Y. Fang, J. Li, *Adv. Funct. Mater.* **2018**, *28*, 1705593.
[24] J.-L. Qi, J. Wu, S.-F. Yan, J.-J. Xu, W. Liu, S.-P. Guo, *Inorg. Chem.* **2023**, *62*, 18825.
[25] J. Wu, Y. Guo, J.-L. Qi, W.-D. Yao, S.-X. Yu, W. Liu, S.-P. Guo, *Angewandte Chemie International Edition* **2023**, *62*, e202301937.
[26] Y. Ma, J. Ma, P. Wang, J. Niu, J. Zhang, C. Duan, S. Chen, C. Han, H. Xu, *Science Advances* **2024**, *10*, eadk3983.
[27] S. Fang, A. Du, B. Zhou, Z. Liu, J. Nie, Y. Wang, H. Zhong, H. Hu, H. Li, Y. Shi, *Adv. Opt. Mater. Multimode Ratio Fluorescence* **2023**, *11*, 2202952.
[28] Z. Ma, S. Yang, Y. Shi, Y. Fu, K. Wang, G. Xiao, B. Zou, *Angewandte Chemie International Edition* **2024**, *63*, e202406015.
[29] S. Zhou, Y. Chen, K. Li, X. Liu, T. Zhang, W. Shen, M. Li, L. Zhou, R. He, *Chem. Sci.* **2023**, *14*, 5415.
[30] H. Peng, X. Wang, Y. Tian, B. Zou, F. Yang, T. Huang, C. Peng, S. Yao, Z. Yu, Q. Yao, G. Rao, J. Wang, *ACS Appl. Mater. Interfaces* **2021**, *13*, 13443.
[31] L. Lian, S. Wang, H. Ding, G. Liang, Y.-B. Zhao, H. Song, X. Lan, J. Gao, R. Chen, D. Zhang, J. Zhang, *Advanced Optical Materials* **2022**, *10*, 2101640.
[32] H. Peng, Y. Tian, X. Wang, T. Huang, Z. Yu, Y. Zhao, T. Dong, J. Wang, B. Zou, *ACS Appl. Mater. Interfaces* **2022**, *14*, 12395.
[33] L. Lian, P. Zhang, G. Liang, S. Wang, X. Wang, Y. Wang, X. Zhang, J. Gao, D. Zhang, L. Gao, H. Song, R. Chen, X. Lan, W. Liang, G. Niu, J. Tang, J. Zhang, *ACS Appl. Mater. Interfaces* **2021**, *13*, 22749.
[34] W. Meng, C. Wang, Y. Li, G. Hu, S. Sui, G. Xu, M. Peng, Z. Deng, *Chemistry – A European Journal* **2023**, *29*, e202202675.
[35] M. Xie, C. Han, J. Zhang, G. Xie, H. Xu, *Chem. Mater.* **2017**, *29*, 6606.
[36] F. Farinella, L. Maini, P. P. Mazzeo, V. Fattori, F. Monti, D. Braga, *Dalton Trans.* **2016**, *45*, 17939.

[37] J. Chen, S. Geng, X. Zhang, X. Pan, C. Chen, R. Li, J. Wen, C. Sun, R. Chen, Z. Xiao, L. Mao, *ACS Materials Lett.* **2024**, *6*, 865.
[38] Y. Fang, W. Liu, S. J. Teat, G. Dey, Z. Shen, L. An, D. Yu, L. Wang, D. M. O'Carroll, J. Li, *Adv. Funct. Mater.* **2017**, *27*, 1603444.
[39] J. Troyano, F. Zamora, S. Delgado, *Chem. Soc. Rev.* **2021**, *50*, 4606.
[40] P. C. Ford, E. Cariati, J. Bourassa, *Chem. Rev.* **1999**, *99*, 3625.
[41] M. R. Churchill, K. L. Kalra, *Inorg. Chem.* **1974**, *13*, 1065.
[42] C. Chen, R.-H. Li, B.-S. Zhu, K.-H. Wang, J.-S. Yao, Y.-C. Yin, M.-M. Yao, H.-B. Yao, S.-H. Yu, *Angew. Chem. Int. Ed.* **2018**, *57*, 7106.
[43] X. Ji, Y. Liu, R. Li, Z. Zhang, X. Zhang, C. Chen, J. Chen, H. Lu, R. Chen, L. Mao, *Advanced Optical Materials* **2023**, *11*, 2300541.
[44] H. Miao, Y. Zhou, P. Wang, Z. Huang, W. Zhaxi, L. Liu, F. Duan, J. Wang, X. Ma, S. Jiang, W. Huang, Q. Zhang, D. Wu, *Chem. Commun.* **2023**, *59*, 1229.
[45] N. Zhang, H. Hu, L. Qu, R. Huo, J. Zhang, C. Duan, Y. Meng, C. Han, H. Xu, *J. Am. Chem. Soc.* **2022**, *144*, 6551.
[46] S. Wang, E. E. Morgan, S. Panuganti, L. Mao, P. Vishnoi, G. Wu, Q. Liu, M. G. Kanatzidis, R. D. Schaller, R. Seshadri, *Chem. Mater.* **2022**, *34*, 3206.
[47] B. Wang, Y. Fu, Y. Shen, P. Wang, Y. Chen, F. Feng, Z. Xu, W. Huang, D. Wu, *Inorg. Chem.* **2024**, *63*, 8070.
[48] B. Huitorel, H. El Moll, R. Utrera-Melero, M. Cordier, A. Fargues, A. Garcia, F. Massuyeau, C. Martineau-Corcos, F. Fayon, A. Rakhmatullin, S. Kahlal, J.-Y. Saillard, T. Gacoin, S. Perruchas, *Inorg. Chem.* **2018**, *57*, 4328.
[49] M. Xie, C. Han, Q. Liang, J. Zhang, G. Xie, H. Xu, *Sci. Adv.* **2019**, *5*, eaav9857.
[50] P. Suomalainen, H. K. Reinius, H. Riihimäki, R. H. Laitinen, S. Jääskeläinen, M. Haukka, J. T. Pursiainen, T. A. Pakkanen, A. O. I. Krause, *Journal of Molecular Catalysis A: Chemical* **2001**, *169*, 67.
[51] S. Perruchas, C. Tard, X. F. Le Goff, A. Fargues, A. Garcia, S. Kahlal, J.-Y. Saillard, T. Gacoin, J.-P. Boilot, *Inorg. Chem.* **2011**, *50*, 10682.
[52] A. Bondi, *J. Phys. Chem.* **1964**, *68*, 441.
[53] S. Sculfort, P. Braunstein, *Chem. Soc. Rev.* **2011**, *40*, 2741.
[54] R. K. Harris, A. C. Olivieri, *Progress in Nuclear Magnetic Resonance Spectroscopy* **1992**, *24*, 435.
[55] B. Huitorel, H. El Moll, R. Utrera-Melero, M. Cordier, A. Fargues, A. Garcia, F. Massuyeau, C. Martineau-Corcos, F. Fayon, A. Rakhmatullin, S. Kahlal, J.-Y. Saillard, T. Gacoin, S. Perruchas, *Inorg. Chem.* **2018**, *57*, 4328.
[56] B. Huitorel, R. Utrera-Melero, F. Massuyeau, J.-Y. Mevelec, B. Baptiste, A. Polian, T. Gacoin, C. Martineau-Corcos, S. Perruchas, *Dalton Trans.* **2019**, *48*, 7899.
[57] Q. Benito, X. F. Le Goff, G. Nocton, A. Fargues, A. Garcia, A. Berhault, S. Kahlal, J.-Y. Saillard, C. Martineau, J. Trébosc, T. Gacoin, J.-P. Boilot, S. Perruchas, *Inorg. Chem.* **2015**, *54*, 4483.
[58] G. A. Bowmaker, P. C. Healy, *Spectrochimica Acta Part A: Molecular Spectroscopy* **1988**, *44*, 115.
[59] R. Utrera-Melero, B. Huitorel, M. Cordier, J.-Y. Mevellec, F. Massuyeau, C. Latouche, C. Martineau-Corcos, S. Perruchas, *Inorg. Chem.* **2020**, *59*, 13607.
[60] S. Attar, J. H. Nelson, *Inorg. Chem.* **1991**, *30*, 4143.
[61] R. Utrera-Melero, M. Cordier, F. Massuyeau, J.-Y. Mevellec, A. Rakhmatullin, C. Martineau-Corcos, C. Latouche, S. Perruchas, *Inorg. Chem.* **2023**, *62*, 18157.
[62] Q. Benito, X. F. Le Goff, S. Maron, A. Fargues, A. Garcia, C. Martineau, F. Taulelle, S. Kahlal, T. Gacoin, J.-P. Boilot, S. Perruchas, *J. Am. Chem. Soc.* **2014**, *136*, 11311.
[63] S. Perruchas, C. Tard, X. F. Le Goff, A. Fargues, A. Garcia, S. Kahlal, J.-Y. Saillard, T. Gacoin, J.-P. Boilot, *Inorg. Chem.* **2011**, *50*, 10682.
[64] H. Kitagawa, Y. Ozawa, K. Toriumi, *Chem. Commun.* **2010**, *46*, 6302.
[65] X.-C. Shan, F.-L. Jiang, H. Zhang, X.-Y. Qian, L. Chen, M.-Y. Wu, S. A. AL-Thabaiti, M.-C. Hong, *Chem. Commun.* **2013**, *49*, 10227.
[66] C. D. S. Brites, A. Millán, L. D. Carlos, In *Handbook on the Physics and Chemistry of Rare Earths* (Eds.: Jean-Claude, B.; Vitalij K., P.), Elsevier, **2016**, pp. 339–427.

[67] Z. Wang, S. Yu, H. Zhang, H. Duan, *Synthetic Metals* **2019**, *255*, 116104.
[68] A. V. Shamsieva, I. E. Kolesnikov, I. D. Strelnik, T. P. Gerasimova, A. A. Kalinichev, S. A. Katsyuba, E. I. Musina, E. Lähderanta, A. A. Karasik, O. G. Sinyashin, *J. Phys. Chem. C* **2019**, *123*, 25863.
[69] J. Zhang, Y. Li, S. Liu, J. Lin, Y.-N. Fan, Z. Li, *European Journal of Inorganic Chemistry* **2023**, *26*, e202300595.
[70] J.-H. Wang, M. Li, J. Zheng, X.-C. Huang, D. Li, *Chem. Commun.* **2014**, *50*, 9115.
[71] D. Cauzzi, R. Pattacini, M. Delferro, F. Dini, C. Di Natale, R. Paolesse, S. Bonacchi, M. Montalti, N. Zaccheroni, M. Calvaresi, F. Zerbetto, L. Prodi, *Angew. Chem. Int. Ed.* **2012**, *51*, 9662.
[72] Y. Li, Z. Li, Y. Hou, Y.-N. Fan, C.-Y. Su, *Inorg. Chem.* **2018**, *57*, 13235.
[73] Y. Cheng, Y. Gao, H. Lin, F. Huang, Y. Wang, *J. Mater. Chem. C* **2018**, *6*, 7462.
[74] R. Utrera-Melero, J. Mevellec, N. Gautier, N. Stephant, F. Massuyeau, S. Perruchas, *Chem. Asian J.* **2019**, *14*, 3166.